

Article

# Two Dimensional Magnetic Coordination Polymers Formed by Lanthanoids and Chlorocyananilato<sup>†</sup>

Samia Benmansour \*, Antonio Hernández-Paredes and Carlos J. Gómez-García \* 

Instituto de Ciencia Molecular (ICMol), Departamento de Química Inorgánica, Universidad de Valencia, C/Catedrático José Beltrán 2, 46980 Paterna, Spain; anherpa@alumni.uv.es

\* Correspondence: sam.ben@uv.es (S.B.); carlos.gomez@uv.es (C.J.G.-G.);

Tel.: +34-963-544-423 (S.B. & C.J.G.-G.); Fax: +34-963-543-273 (S.B. & C.J.G.-G.)

† In memory of late Professor Samiran Mitra. A good researcher, a better friend and an excellent person.

Received: 8 November 2018; Accepted: 6 December 2018; Published: 12 December 2018



**Abstract:** Here we show the important role played by the size of the lanthanoid and the solvent used in the final structures of several two-dimensional magnetic coordination polymers with the ligand chlorocyananilato,  $(C_6O_4(CN)Cl)^{2-}$ . With this aim we have prepared five compounds:  $[Nd_2(C_6O_4(CN)Cl)_3(DMF)_6]$  (**1**) (DMF = dimethylformamide),  $[Dy_2(C_6O_4(CN)Cl)_3(DMF)_6] \cdot 4H_2O$  (**2**),  $[Ho_2(C_6O_4(CN)Cl)_3(DMF)_6] \cdot 2H_2O$  (**3**), and  $[Ln_2(C_6O_4(CN)Cl)_3(DMSO)_6]$  with Ln = Ce (**4**) and Nd (**5**) (DMSO = dimethylsulfoxide). These compounds are formed by two dimensional networks with a (6,3)-topology but, depending on the size of the lanthanoid and on the solvent used, show important structural differences, including the size, shape, distortion and content of the cavities as well as the flatness of the layers. The comparison of compounds **1–3** and **4–5** shows the role played by the size of the lanthanoid while keeping constant the solvent, whereas, the comparison of compounds **1** and **5** shows the role of the solvent (DMF vs. DMSO) while keeping constant the lanthanoid. The magnetic properties of all of them show the absence of noticeable magnetic interactions, in agreement with previous results that can be explained by the internal character of the 4f electron and the weak magnetic coupling mediated by these anilato-based ligands.

**Keywords:** magnetic coordination polymers; lanthanoids; anilato-based compounds; chlorocyananilato; honeycomb layers; magnetic properties

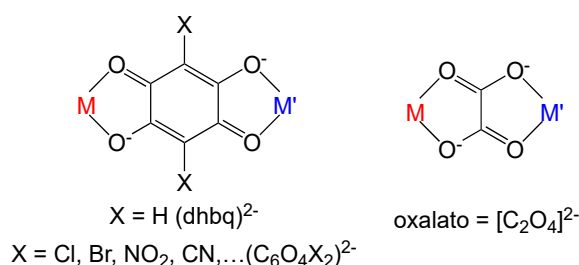
## 1. Introduction

The synthesis of porous crystalline coordination polymers also known as metal organic frameworks (MOFs) presenting different cavities shapes and sizes is a hot topic in Coordination Chemistry nowadays [1,2]. The possibility to tune and modulate the shape and size of the cavities is a very important aspect in order to synthesize MOFs with tailored properties for applications in catalysis [3,4], gas storage and separation [5,6], energy storage [7,8], water adsorption [9], biomedicine [10,11], sensors [12,13], or a combination of several properties in the same MOF [14].

These MOFs are mainly constructed with transition metal atoms (including group 12) and complexes of these metal ions that are connected through different organic ligands acting as linkers. Although less used, lanthanides can also be used to prepare MOFs with interesting properties as luminescence in order to prepare optical-based sensors of gases, contaminants and different chemical species [15–17].

Although there are hundreds of organic ligands that can be used as linkers, the most popular ones are polycarboxylic acids (including aromatic) [14,18–21], and azolates [22,23] thanks to their capacity to coordinate many transition metal atoms (and lanthanoids) with diverse coordination modes. Aromatic quinones as the 2,5-dihydroxy-1,4-benzoquinone dianion  $(C_6O_4H_2)^{2-}$  = dhbq and the 3,6-disubstituted

dianions  $(C_6O_4X_2)^{2-}$  (anilato-type ligands) with  $X = CN/Cl, NO_2, Br, Cl, CN, \dots$  (Scheme 1) have also been used to prepare MOFs with interesting magnetic properties [24,25]. One of the interests of these anilato derivatives is their topological resemblance with the extensively studied oxalato ligand (Scheme 1). Thus, anilato ligands form tris-quelate chiral monomers of the type  $[M(C_6O_4X_2)_3]^{3-}$  [26,27], that resemble the well-known  $[M(C_2O_4)_3]^{3-}$  chiral complexes. Furthermore, anilato ligands also form extended 1D, 2D and 3D lattices with the same topology that oxalate [24,28–33]. Albeit, the anilato ligands present some interesting properties and advantages when compared with oxalato: (i) they are much larger and accordingly, their compounds usually present much larger cavities and channels (in fact, most structures with oxalato are not considered MOFs since they are not porous, in contrast to the equivalent anilato-based compounds) [28,34]. (ii) A second advantage is the possibility to modulate the electron density in the anilato ring by simply changing the X group (Scheme 1). This change in X leads to changes in the cavity sizes (since X points to the centre of the cavity) and, most importantly, in the ordering temperatures of magnetic MOFs as in the series of anilato-based magnets  $[(H_3O)(phz)_3][MnCr(C_6O_4X_2)_3] \cdot G$  ( $phz = \text{phenazine}$ ;  $X = H, Cl, Br$  and  $I$ ,  $G = H_2O$  or acetone) [30].



**Scheme 1.** (left) bis-bidentate coordination mode of the anilato-type ligands and of the oxalato ligand (right).

Besides transition metal ions, lanthanoids have also been used to prepare anilato-based neutral lattices formulated as  $[Ln_2(C_6O_4X_2)_3(G)_m] \cdot nG$  whose structure depends on the size of the Ln(III) ion, the X group and the solvent used (G).

The ligand  $C_6O_4H_2^{2-} = \text{dhbq}^{2-}$  with  $G = H_2O$  was used by Robson et al. [28,35] and later by some of us [36] to prepare the complete series of isostructural compounds formulated as  $[Ln_2(C_6O_4H_2)_3(H_2O)_6] \cdot 18H_2O$ . In this series all the Ln(III) present the same structure: a (6,3)-2D honeycomb lattice formed by regular non planar hexagons with the Ln(III) ions nona-coordinated with a tri-capped trigonal prismatic geometry.

For the ligand  $C_6O_4Cl_2^{2-} = \text{chloranilato}$  and  $G = H_2O$ , the change of the Ln(III) size leads to four different crystal phases, all based in the (6,3)-2D honeycomb lattice with formula  $[Ln_2(C_6O_4Cl_2)_3(H_2O)_6] \cdot nH_2O$ . These four phases (I-IV) only differ in the disposition of the coordinated water molecules around the Ln(III) ions, due to the change in the Ln(III) size. This change in the coordination environment results in important changes in the number of crystallization water molecules located in the cavities:  $n = 14$ , for the larger Ln(III) ions (La, Ce, Pr and Nd) in phase I,  $n = 12$  for the intermediate Ln(III) (Sm, Eu, Gd, Tb, Dy and Ho) in phase II,  $n = 10$  for Ln = Er(III) in phase III and finally,  $n = 8$  for the smallest lanthanoids (Tm and Yb) in phase IV [28,35,36].

With the ligand  $C_6O_4Br_2^{2-} = \text{bromanilato}$  and  $G = H_2O$ , we have obtained two different crystallographic phases (I and II), also depending on the size of the Ln(III) ion. These phases, formulated as  $[Ln_2(C_6O_4Br_2)_3(H_2O)_6] \cdot nH_2O$ , are also based on the (6,3)-2D honeycomb lattice and contain 12 crystallization  $H_2O$  molecules for the larger Ln(III) ions (La to Er, phase I) or 8 water molecules for the smallest ions (Yb and Tm, phase II). These two phases also differ in the disposition of the water molecules and in the spatial orientation of the bromanilato ligands [36,37].

For the nitrilanilato ligand ( $X = NO_2$ ), the larger size of the nitro group compared to H, Cl and Br prevented, in our case, the formation of the (6,3)-2D honeycomb lattice and led to the formation of nitrilanilato-bridged dimers formulated as  $[Ln_2(C_6O_4(NO_2)_2)_3(H_2O)_{10}] \cdot 6H_2O$  although only for the intermediate Ln(III) ions (Sm-Er) [36,38].

Finally, the asymmetric chlorocyananilato ligand ( $C_6O_4(CN)Cl^{2-}$ ) has very recently been used with Dy(III) and  $H_2O$  to prepare compound  $[H_3O][Dy(C_6O_4(CN)Cl)_2(H_2O)] \cdot 4H_2O$  that presents a very unusual square (4,4)-2D lattice [39].

All these previous results have been obtained using water as solvent. In fact, until very recently, the only example obtained with other solvent was compound  $[Pr_2(C_6O_4Cl_2)_3(EtOH)_6] \cdot 2EtOH$ , that also presents a structure based on the (6,3)-2D honeycomb lattice although with very large distortions of the hexagonal cavities that appear as rectangles [40]. In the last two years our group has prepared a number of anilato-based Ln(III) compounds using different solvents with high coordinating capacity towards Ln(III) ions [41]. These studies include compounds as  $[Er_2(C_6O_4Br_2)_3(DMSO)_4] \cdot 2DMSO \cdot 2H_2O$  and  $[Er_2(C_6O_4Br_2)_3(DMF)_6]$  [37] that present the same (6,3)-2D topology but with rectangular cavities (in the DMF compound) or very distorted hexagonal ones (in the DMSO compound) and with a coordination number of eight (compared to nine for the  $H_2O$  derivative). A larger study of the role of the solvent performed with the chloranilato ligand and Er(III) in the series of compounds  $[Er_2(C_6O_4Cl_2)_3(H_2O)_6] \cdot 10H_2O$ ,  $[Er_2(C_6O_4Cl_2)_3(DMF)_6]$ ,  $[Er_2(C_6O_4Cl_2)_3(DMA)_4] \cdot 5H_2O$  (DMA = dimethylacetamide),  $[Er_2(C_6O_4Cl_2)_3(DMSO)_4] \cdot 2DMSO \cdot 2H_2O$ ,  $[Er_2(C_6O_4Cl_2)_3(FMA)_6] \cdot 4FMA \cdot 2H_2O$  (FMA = formamide) and  $[Er_2(C_6O_4Cl_2)_3(HMPA)(H_2O)_3] \cdot H_2O$  (HMPA = hexamethylphosphoramide) showed that the size and steric hindrance of the solvent determines the coordination number and geometry, the size and shape of the cavities and, accordingly, the presence of solvent and water molecules in the cavities [42]. All these results indicate that the solvent plays a very important role in the final structure. Very recently we have also prepared a series formulated as:  $[Ln_2(C_6O_4Br_2)_3(DMSO)_n] \cdot 2DMSO \cdot mH_2O$  with  $n = 6$  and  $m = 0$  for  $Ln = La-Gd$  and  $n = 4$  and  $m = 2$  for  $Ln = Tb-Yb$  [43]. In this series, as previously observed in the series  $[Ln_2(C_6O_4X_2)_3(H_2O)_6] \cdot nH_2O$  ( $X = Cl, Br$  and  $NO_2$ ), the size of the Ln(III) ion plays a key structural role. Finally, also very recently, we have combined the asymmetric chlorocyananilato ligand,  $(C_6O_4(CN)Cl)^{2-}$ , with different Ln(III) ions as Ce(III), Pr(III) and Yb(III) using DMF and DMSO as solvents to prepare the compounds  $[Ce_2(C_6O_4(CN)Cl)_3(DMF)_6] \cdot 2H_2O$  (I),  $[Pr_2(C_6O_4(CN)Cl)_3(DMF)_6]$  (II),  $[Pr_2(C_6O_4(CN)Cl)_3(DMSO)_6]$  (III) and  $[Yb_2(C_6O_4(CN)Cl)_3(DMSO)_4] \cdot 2H_2O$  (IV) [39]. These four compounds showed some hints about the role of the solvent and the size of the Ln(III) in the final structure, but, given the reduced number of compounds did not allow to extract deeper conclusions.

Here we extend this study with the asymmetric chlorocyananilato ligand and dimethylformamide (DMF) and dimethylsulfoxide (DMSO) as solvents with four more Ln(III) ions (Ce, Nd, Dy and Ho) to prepare five new compounds formulated as:  $[Nd_2(C_6O_4(CN)Cl)_3(DMF)_6]$  (1)  $[Dy_2(C_6O_4(CN)Cl)_3(DMF)_6] \cdot 4H_2O$  (2),  $[Ho_2(C_6O_4(CN)Cl)_3(DMF)_6] \cdot 2H_2O$  (3), and  $[Ln_2(C_6O_4(CN)Cl)_3(DMSO)_6]$  with  $Ln = Ce$  (4) and  $Nd$  (5). These five compounds, together with the four compounds previously reported with the same ligand and identical stoichiometry:  $[Ce_2(C_6O_4(CN)Cl)_3(DMF)_6] \cdot 2H_2O$  (I),  $[Pr_2(C_6O_4(CN)Cl)_3(DMF)_6]$  (II),  $[Pr_2(C_6O_4(CN)Cl)_3(DMSO)_6]$  (III) and  $[Yb_2(C_6O_4(CN)Cl)_3(DMSO)_4] \cdot 2H_2O$  (IV) [39] will allow us to obtain a deeper knowledge of the role played by both factors: the size of the Ln(III) ion and the solvent (DMF and DMSO) with the asymmetric ligand chlorocyananilato.

## 2. Results and Discussion

### 2.1. Syntheses of the Complexes

Compounds 1 and 2 were synthesized by carefully layering solutions containing the Ln(III) ion, dissolved in DMF, and the asymmetric chlorocyananilato ligand, as its tetraphenylphosphonium salt, dissolved in methanol. Compounds 3–5 were synthesized in the same way but using the monopotassium salt of the asymmetric chlorocyananilato ligand dissolved in the corresponding solvent: DMF (for 3) and DMSO (for 4 and 5). As expected, given the strong affinity towards Ln(III) ions of the used solvents (DMF and DMSO) [41], they appear in all cases coordinated to the Ln(III)

ions. The used synthetic method allowed a slow diffusion of the reagents that resulted in good quality single crystals for the determination of the X-ray structure in all cases.

## 2.2. X-ray Power Diffraction (XRPD)

All the samples were analyzed by XRPD to confirm the isostructurality with the solved structures and the phase purity. In all cases the experimental diffractograms are similar to the simulated ones from the single crystal X-ray structure (see supporting information, Figures S1–S5), although the crystallinity of compounds **2** and **3** is very poor due to the loss of the water crystallization molecules.

## 2.3. IR Spectroscopy

The IR spectra of the five compounds show the expected bands attributed to the ligands and the coordinated solvent molecules (see supporting information, Figures S6–S10 and Table S1).

## 2.4. Description of the Structures

**Structure of  $[\text{Nd}_2(\text{C}_6\text{O}_4(\text{CN})\text{Cl})_3(\text{DMF})_6]$  (**1**).** Compound **1** crystallizes in the monoclinic  $P2_1/n$  space group (Table 1). The asymmetric unit (Figure 1a) contains one Nd(III) ion, three coordinated DMF molecules and one and a half chlorocyananilato ligands. This asymmetric unit corresponds to the formula  $[\text{Nd}_2(\text{C}_6\text{O}_4(\text{CN})\text{Cl})_3(\text{DMF})_6]$ . There is an inversion centre in the centre of one of the anilato rings that generates a disorder between the CN and Cl groups with occupancies of  $\frac{1}{2}$  in each position.

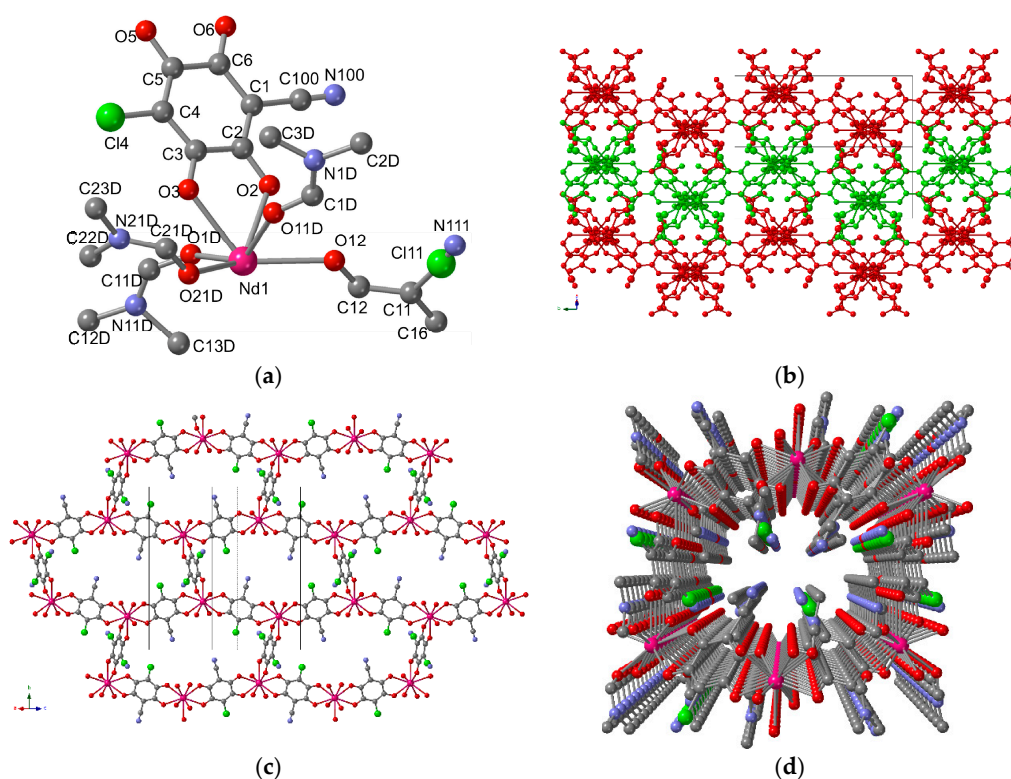


**Figure 1.** (a) Asymmetric unit of compound **1** with the labelling scheme. (b) Side view of the corrugated layers in compound **1**. Consecutive layers are coloured in green and red for clarity. (c) View of a layer in **1** (For the dimethylformamide (DMF) molecules only the oxygen atoms are shown). (d) Perspective view of one rectangular channel along the  $[101]$  direction in compound **1**. Colour code: Nd = pink, Cl = green, C = grey, O = red, N = dark blue. H atoms have been omitted for clarity.

**Table 1.** Crystal data and structure refinement of compounds [Nd<sub>2</sub>(C<sub>6</sub>O<sub>4</sub>(CN)Cl)<sub>3</sub>(DMF)<sub>6</sub>] (1), [Dy<sub>2</sub>(C<sub>6</sub>O<sub>4</sub>(CN)Cl)<sub>3</sub>(DMF)<sub>6</sub>]·4H<sub>2</sub>O (2), [Ho<sub>2</sub>(C<sub>6</sub>O<sub>4</sub>(CN)Cl)<sub>3</sub>(DMF)<sub>6</sub>]·2H<sub>2</sub>O (3) and [Ln<sub>2</sub>(C<sub>6</sub>O<sub>4</sub>(CN)Cl)<sub>3</sub>(DMSO)<sub>6</sub>] with Ln = Ce (4) and Nd (5).

	1	2	3	4	5
Formula	C <sub>39</sub> H <sub>42</sub> Cl <sub>3</sub> N <sub>9</sub> O <sub>18</sub> Nd <sub>2</sub>	C <sub>39</sub> H <sub>50</sub> Cl <sub>3</sub> N <sub>9</sub> O <sub>22</sub> Dy <sub>2</sub>	C <sub>39</sub> H <sub>46</sub> Cl <sub>3</sub> N <sub>9</sub> O <sub>20</sub> Ho <sub>2</sub>	C <sub>33</sub> H <sub>36</sub> Cl <sub>3</sub> N <sub>3</sub> O <sub>18</sub> S <sub>6</sub> Ce <sub>2</sub>	C <sub>33</sub> H <sub>36</sub> Cl <sub>3</sub> N <sub>3</sub> O <sub>18</sub> S <sub>6</sub> Nd <sub>2</sub>
F. Wt.	1319.64	1428.22	1397.05	1341.63	1349.88
Space group (#)	<i>P</i> 2 <sub>1</sub> / <i>n</i> (14)	<i>C</i> 2/ <i>c</i> (15)	<i>C</i> 2/ <i>c</i> (15)	<i>P</i> 2 <sub>1</sub> / <i>n</i> (14)	<i>P</i> 2 <sub>1</sub> / <i>n</i> (14)
Crystal system	Monoclinic	Monoclinic	Monoclinic	Monoclinic	Monoclinic
<i>a</i> (Å)	10.5126(5)	13.6849(3)	13.8612(6)	9.5974(2)	9.6212(3)
<i>b</i> (Å)	18.8316(10)	22.8267(6)	23.0470(10)	16.4105(3)	16.3828(4)
<i>c</i> (Å)	12.7477(5)	17.7221(4)	17.9615(8)	15.3719(3)	15.2790(3)
$\alpha$ (°)	90	90	90	90	90
$\beta$ (°)	97.445(5)	98.349(2)	98.363(4)	91.111(2)	91.989
$\gamma$ (°)	90	90	90	90	90
<i>V</i> /Å <sup>3</sup>	2502.4(2)	5477.4(2)	5676.9(4)	2420.59(8)	2406.86(11)
<i>Z</i>	2	4	4	2	2
<i>T</i> (K)	120	120	120	120	120
$\rho_{\text{calc}}$ /g cm <sup>-3</sup>	1.751	1.722	1.630	1.791	1.812
$\mu$ /mm <sup>-1</sup>	2.291	2.936	2.983	2.351	2.630
<i>F</i> (000)	1308	2792	2736	1252	1260
<i>R</i> (int)	0.0558	0.0283	0.0207	0.0302	0.0573
$\theta$ range (deg)	3.400–25.040	3.360–25.035	3.324–25.045	3.267–28.009	3.267–25.036
Total reflections	9854	10265	11058	9482	15285
Unique reflections	4419	4835	5005	4858	4251
Data with <i>I</i> > 2 $\sigma$ ( <i>I</i> )	3048	4155	4527	4062	3221
<i>N</i> <sub>var</sub>	334	352	361	338	347
<i>R</i> <sub>1</sub> <sup>a</sup> on <i>I</i> > 2 $\sigma$ ( <i>I</i> )	0.0718	0.0376	0.0296	0.0612	0.0553
<i>wR</i> <sub>2</sub> <sup>b</sup> (all)	0.1808	0.0988	0.0767	0.1509	0.1375
GOF <sup>c</sup> on <i>F</i> <sup>2</sup>	1.061	1.041	1.078	1.066	1.029
$\Delta\rho_{\text{max}}$ (eÅ <sup>-3</sup> )	1.644	1.354	0.836	2.088	2.424
$\Delta\rho_{\text{min}}$ (eÅ <sup>-3</sup> )	−1.581	−1.021	−0.561	−1.314	−1.216

$$^a R_1 = \sum ||F_o| - |F_c|| / \sum |F_o|. \quad ^b wR_2 = [\sum w(F_o^2 - F_c^2)^2 / \sum w(F_o^2)^2]^{1/2}. \quad ^c \text{GOF} = [\sum [w(F_o^2 - F_c^2)^2 / (N_{\text{obs}} - N_{\text{var}})]^{1/2}.$$

The structure of **1** presents corrugated layers parallel to the (10-1) plane (Figure 1b) with a (6,3)-2D honeycomb topology (Figure 1c) where the hexagons are so distorted that they can rather be described as parallel rectangles packed in a brick-wall mode (Figure 1c). The large distortions of the cavities are evidenced by the three Nd-Nd distances along the diagonals of the cavities (21.63(4), 17.54(2) and 12.030(2) Å) and by the corresponding Nd-Nd-Nd angles (85.10°, 114.53° and 157.90°). The rectangles are formed by six Nd(III) centres in the vertex connected through bis-bidentate chlorocyananilato bridges in the sides. When viewed along the [100] direction, the layers form rectangular channels although with very little empty space (Figure 1d).

The coordination environment around the Nd(III) ions is a capped square anti-prism geometry (see below) formed by three chelate chlorocyananilato ligands and three oxygen atoms from three DMF molecules (Figure 1a). The Nd-O bond distances (Table 2) are similar to those observed in the related Nd-containing anilato-based compounds: [Nd<sub>2</sub>(C<sub>6</sub>O<sub>4</sub>X<sub>2</sub>)<sub>3</sub>(H<sub>2</sub>O)<sub>6</sub>]·*n*H<sub>2</sub>O (X = H, *n* = 18; X = Cl, *n* = 14 and X = Br, *n* = 12) [28,36] and in [Nd<sub>2</sub>(C<sub>6</sub>O<sub>4</sub>Br<sub>2</sub>)<sub>3</sub>(DMSO)<sub>6</sub>]·2DMSO [43]. As expected, the Nd-O<sub>anilato</sub> bond distances are longer than the Nd-O<sub>DMF</sub> ones due to the chelating coordination mode of the chlorocyananilato ligand.

**Structure of [Ln<sub>2</sub>(C<sub>6</sub>O<sub>4</sub>(CN)Cl)<sub>3</sub>(DMF)<sub>6</sub>]·*n*H<sub>2</sub>O; Ln = Dy, *n* = 4 (2) and Ln = Ho, *n* = 2 (3).** Compounds **2** and **3** are isostructural and both crystallize in the monoclinic *C*2/*c* space group (Table 1). Given the similarity between both structures, we will only describe the structure of compound **2** although we will compare all the structures in detail below. The asymmetric unit of **2** (Figure 2a) contains one Dy(III) ion (Ho(III) in **3**), three coordinated DMF molecules, three halves chlorocyananilato

ligands and two crystallization water molecules (three water molecules with occupancy 1/3 in compound **3**). This asymmetric unit corresponds to the formula  $[\text{Ln}_2(\text{C}_6\text{O}_4(\text{CN})\text{Cl})_3(\text{DMF})_6] \cdot n\text{H}_2\text{O}$  with  $\text{Ln} = \text{Dy}$ ,  $n = 4$  in **2** and  $\text{Ln} = \text{Ho}$ ,  $n = 2$  in **3**. There is an inversion centre in the centre of the three anilato rings that generates a disorder between the CN and Cl groups with occupancies of  $\frac{1}{2}$  each.

**Table 2.** Bond distances (Å) for compounds  $[\text{Nd}_2(\text{C}_6\text{O}_4(\text{CN})\text{Cl})_3(\text{DMF})_6]$  (**1**),  $[\text{Dy}_2(\text{C}_6\text{O}_4(\text{CN})\text{Cl})_3(\text{DMF})_6] \cdot 4\text{H}_2\text{O}$  (**2**),  $[\text{Ho}_2(\text{C}_6\text{O}_4(\text{CN})\text{Cl})_3(\text{DMF})_6] \cdot 2\text{H}_2\text{O}$  (**3**) and  $[\text{Ln}_2(\text{C}_6\text{O}_4(\text{CN})\text{Cl})_3(\text{DMSO})_6]$  with  $\text{Ln} = \text{Ce}$  (**4**) and  $\text{Nd}$  (**5**).

Bond <sup>a</sup>	1	2	3	4	5
Ln-O2	2.513(7)	2.444(4)	2.407(3)	2.571(5)	2.512(5)
Ln-O3	2.493(7)	2.439(4)	2.497(3)	2.556(5)	2.538(5)
Ln-O5	2.513(7)	2.491(4)	2.408(3)	2.572(5)	2.545(5)
Ln-O6	2.510(7)	2.387(4)	2.514(3)	2.596(5)	2.540(6)
Ln-O12	2.498(7)	2.470(4)	2.458(3)	2.554(5)	2.507(5)
Ln-O16	2.518(8)	2.381(3)	2.466(3)	2.567(6)	2.529(6)
<Ln-O#>	2.508	2.454	2.470	2.569	2.529
Ln-O1D	2.440(9)	2.336(4)	2.357(3)	2.436(6)	2.394(6)
Ln-O11D	2.444(8)	2.382(4)	2.407(3)	2.437(6)	2.420(6)
Ln-O21D	2.417(8)	2.371(4)	2.396(3)	2.437(6)	2.391(6)
<Ln-O#D>	2.434	2.363	2.387	2.437	2.402

<sup>a</sup> For compound **2**: O5 = O12, O6 = O13, O12 = O22 and O16 = O23; for compound **3**: O3 = O6, O5 = O12, O6 = O16, O12 = O22 and O16 = O26.

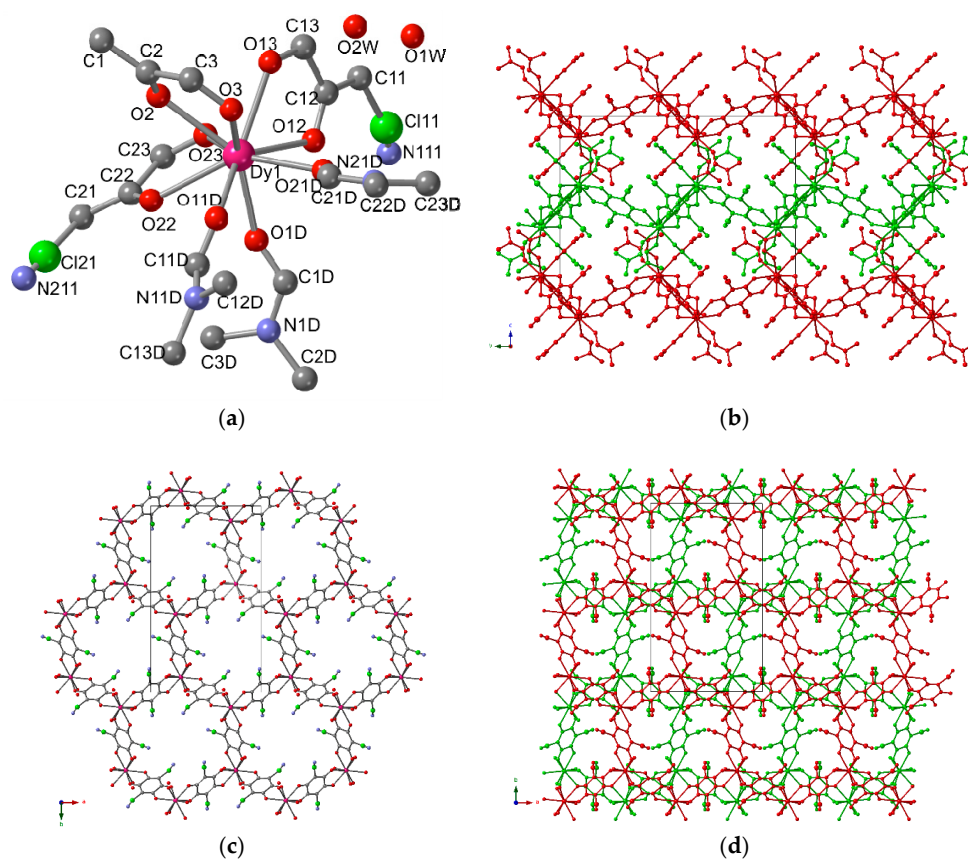


**Figure 2.** (a) Asymmetric unit of compound **2** with the labelling scheme. (b) Side view of the corrugated layers in compound **2**. Consecutive layers are coloured in green and red for clarity. (c) View of a layer in **1**. (d) View of two consecutive layers in **2** showing their alternating disposition. For the DMF molecules only the oxygen atoms are shown in (c,d). Colour code: Dy = pink, Cl = green, C = grey, O = red, N = dark blue. H atoms have been omitted for clarity.

The structure of **2** and **3** shows very corrugated layers parallel to the (10-1) plane (Figure 2b) with a (6,3)-2D honeycomb topology (Figure 2c) with quite regular hexagonal cavities (the Ln-Ln distances are 16.237(7), 16.281(7) and 15.6506(8) Å in **2** and 16.436(13), 16.480(15) and 15.7904(11) Å in **3**). The lack of planarity of these hexagonal cavities is confirmed by the three Ln-Ln-Ln angles inside the hexagon: (98.19°, 98.50° and 101.96° for **2** and 98.15°, 98.46° and 102.23° for **3**). These hexagons contain six Ln(III) ions in the vertex and six bis-bidentate chlorocyananilato bridges in the sides. Consecutive layers are disposed in an alternating way (Figure 2d), precluding the formation of channels. The coordination geometry around the Ln(III) ions can be described as a distorted square anti-prism (see below and Table 3) formed by three chelate chlorocyananilato ligands and three oxygen atoms from three DMF molecules (Figure 2a).

**Table 3.** SHAPE values for the 13 possible coordination geometries found for coordination number nine in compounds [Nd<sub>2</sub>(C<sub>6</sub>O<sub>4</sub>(CN)Cl)<sub>3</sub>(DMF)<sub>6</sub>] (**1**), [Dy<sub>2</sub>(C<sub>6</sub>O<sub>4</sub>(CN)Cl)<sub>3</sub>(DMF)<sub>6</sub>]·4H<sub>2</sub>O (**2**), [Ho<sub>2</sub>(C<sub>6</sub>O<sub>4</sub>(CN)Cl)<sub>3</sub>(DMF)<sub>6</sub>]·2H<sub>2</sub>O (**3**) and [Ln<sub>2</sub>(C<sub>6</sub>O<sub>4</sub>(CN)Cl)<sub>3</sub>(DMSO)<sub>6</sub>] with Ln = Ce (**4**) and Nd (**5**).

Geometry	Symmetry	1	2	3	4	5
EP-9	D <sub>9h</sub>	35.159	36.051	36.078	36.498	36.635
OPY-9	C <sub>8v</sub>	21.266	22.416	22.466	22.477	22.648
HBPY-9	D <sub>7h</sub>	18.045	20.482	20.529	19.269	19.057
JTC-9	C <sub>3v</sub>	14.924	15.489	15.517	15.902	16.172
JCCU-9	C <sub>4v</sub>	9.355	10.612	10.580	10.849	10.831
CCU-9	C <sub>4v</sub>	7.898	9.589	9.561	9.618	9.703
JCSAPR-9	C <sub>4v</sub>	1.637	1.197	1.180	1.741	1.528
<b>CSAPR-9</b>	<b>C<sub>4v</sub></b>	<b>0.507</b>	<b>0.317</b>	<b>0.301</b>	<b>0.846</b>	<b>0.669</b>
JTCTPR-9	D <sub>3h</sub>	3.060	1.971	1.986	2.490	2.386
TCTPR-9	D <sub>3h</sub>	1.162	0.884	0.884	0.934	0.908
JTDIC-9	C <sub>3v</sub>	12.573	13.277	13.250	11.695	12.101
HH-9	C <sub>2v</sub>	12.212	12.507	12.556	11.578	11.696
MFF-9	C <sub>s</sub>	1.280	0.865	0.849	1.088	0.981

EP-9 = Enneagon; OPY-9 = Octagonal pyramid; HBPY-9 = Heptagonal bipyramid; JTC-9 = Triangular cupola (J3) = trivacant cuboctahedron; JCCU-9 = Capped cube (Elongated square pyramid, J8); CCU-9 = Capped cube; JCSAPR-9 = Capped square antiprism (Gyroelongated square pyramid J10); **CSAPR-9 = Capped square antiprism**; JTCTPR-9 = Tricapped trigonal prism (J51); TCTPR-9 = Tricapped trigonal prism; JTDIC-9 = Tridiminished icosahedron (J63); HH-9 = Hula-hoop; MFF-9 = Muffin. The minima values are indicated in bold.

The Ln-O bond distances (Table 2) are similar to those observed in the related Dy and Ho-containing anilato-based compounds: [Ln<sub>2</sub>(C<sub>6</sub>O<sub>4</sub>X<sub>2</sub>)<sub>3</sub>(H<sub>2</sub>O)<sub>6</sub>]·nH<sub>2</sub>O (Ln = Dy and Ho; X = H, n = 18; X = Cl, n = 12 and X = Br, n = 12) [36] in [Ln<sub>2</sub>(C<sub>6</sub>O<sub>4</sub>(NO<sub>2</sub>)<sub>2</sub>)<sub>3</sub>(H<sub>2</sub>O)<sub>10</sub>]·6H<sub>2</sub>O (Ln = Dy and Ho) [36,38] and in [Ln<sub>2</sub>(C<sub>6</sub>O<sub>4</sub>Br<sub>2</sub>)<sub>3</sub>(DMSO)<sub>4</sub>]·2DMSO·2H<sub>2</sub>O (Ln = Dy and Ho) [43]. As observed in compound **1**, the Ln-O<sub>anilato</sub> bond distances are longer than the Ln-O<sub>DMF</sub> ones due to the chelating coordination mode of the chlorocyananilato ligand.

**Structure of [Ln<sub>2</sub>(C<sub>6</sub>O<sub>4</sub>(CN)Cl)<sub>3</sub>(DMSO)<sub>6</sub>], Ln = Ce (**4**) and Nd (**5**).** Compounds **4** and **5** are isostructural and, therefore, we will only describe the structure of compound **4** although we will compare both in detail below. Both compounds crystallize in the monoclinic *P*2<sub>1</sub>/*n* space group (Table 1). The asymmetric unit of **4** (Figure 3a) contains one Ce(III) ion (Nd(III) in **5**), three coordinated DMSO molecules and one and a half chlorocyananilato ligands. This asymmetric unit corresponds to the formula [Ln<sub>2</sub>(C<sub>6</sub>O<sub>4</sub>(CN)Cl)<sub>3</sub>(DMSO)<sub>6</sub>] with Ln = Ce in **4** and Nd in **5**. The presence of an inversion centre in the centre of one anilato rings generates a disorder between the CN and Cl groups with occupancies of  $\frac{1}{2}$  each.

Both compounds show corrugated layers (Figure 3b) with a (6,3)-2D honeycomb topology (Figure 3c) formed by very distorted cavities that look like rectangles. These rectangles are packed in parallel rows in a brick-wall mode (Figure 3c), as observed in compound **1**. The large distortions of the cavities are evidenced by the three Ln-Ln distances along the diagonals of the cavities (20.749(9), 19.439(17) and 11.039(3) Å in **4** and 20.469(10), 19.303(17) and 11.023(3) Å in **5**) and by

the corresponding Ln-Ln-Ln angles ( $91.40^\circ$ ,  $100.67^\circ$  and  $164.41^\circ$  in **4** and  $92.13^\circ$ ,  $100.46^\circ$  and  $163.76^\circ$  in **5**). As in **1**, the rectangles are formed by six Ln(III) centres located in the vertex and by bis-bidentate chlorocyananilato bridges in the sides. These rectangles form channels along the  $[100]$  direction with very little empty space (Figure 3d).

The coordination environment around the Ln(III) ions is a capped square anti-prism geometry (see below and Table 3) formed by three chelate chlorocyananilato ligands and three oxygen atoms from three DMSO molecules (Figure 3a). The Ln-O bond distances (Table 2) are similar to those observed in the related Ce and Nd-containing anilato-based compounds:  $[\text{Ln}_2(\text{C}_6\text{O}_4\text{X}_2)_3(\text{H}_2\text{O})_6] \cdot n\text{H}_2\text{O}$  (Ln = Ce and Nd; X = H,  $n = 18$ ; X = Cl,  $n = 14$  and X = Br,  $n = 12$ ) [28,36] in  $[\text{Ce}_2(\text{C}_6\text{O}_4\text{Br}_2)_3(\text{DMF})_6] \cdot 2\text{H}_2\text{O}$  [39] and in  $[\text{Ln}_2(\text{C}_6\text{O}_4\text{Br}_2)_3(\text{DMSO})_6]$  (Ln = Ce and Nd) [43]. As observed in compounds **1–3**, the Nd-O<sub>anilato</sub> bond distances are longer than the corresponding ones with the solvent molecules (DMSO in **4** and **5**).

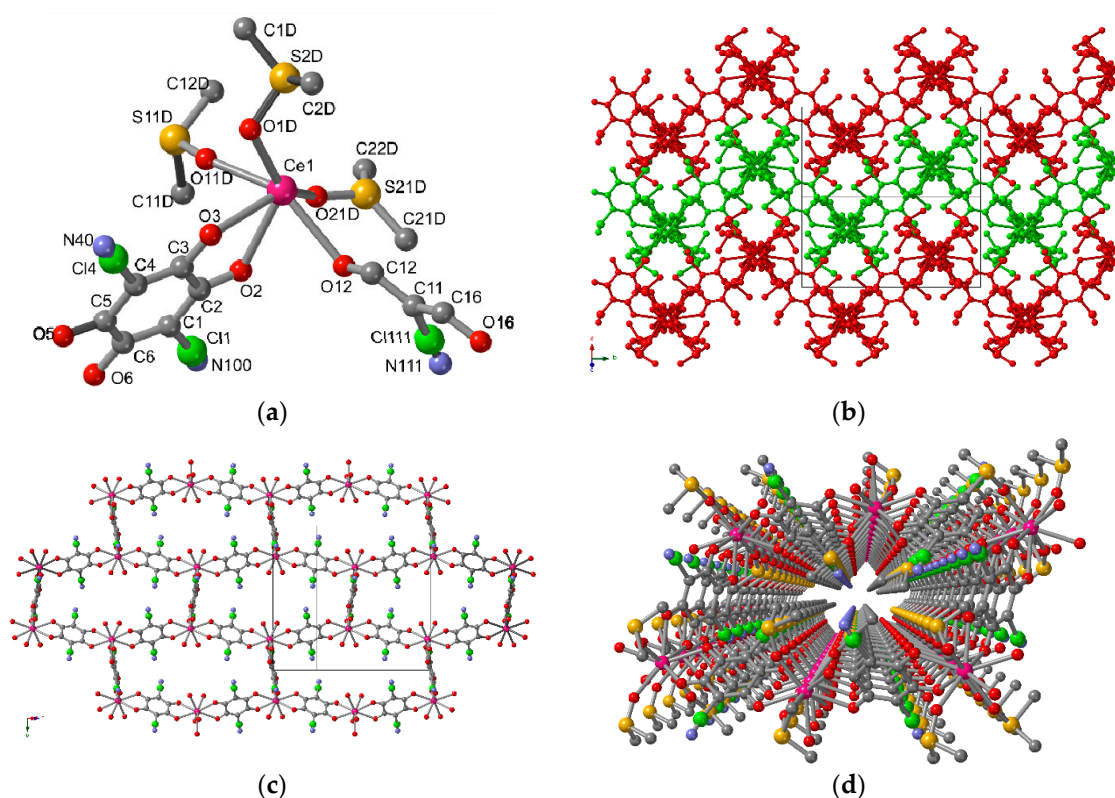


**Figure 3.** (a) Asymmetric unit of compound **4** with the labelling scheme. (b) Side view of the corrugated layers in compound **4**. Consecutive layers are coloured in green and red for clarity. (c) View of a layer in **4** (For the DMSO molecules only the oxygen atoms are shown). (d) Perspective view of one rectangular channel along the  $[100]$  direction in compound **4**. Colour code: Ce = pink, Cl = green, C = grey, O = red, N = dark blue. H atoms have been omitted for clarity.

### 2.5. Comparison of the Structures

In order to compare all the structures we have initially performed the analysis of the coordination geometry around the Ln(III) ions with the program SHAPE [44]. This analysis shows that the polyhedron that best describes the geometry around the Ln(III) ions in compounds **1–5** is a capped square anti-prism (CSAP, Table 3, Figure 4a–e) [45]. Although the five compounds show the same coordination geometry, there are important differences in the spatial disposition of the anilato ligands and the solvent molecules around the Ln(III). Thus, in compound **1** two of the three solvent molecules are located in the lower square face and the third one in the upper square face (Figure 4a) whereas in compounds **2** and **3** the three solvent molecules occupy one of the triangular faces (Figure 4b,c) and in compounds **4** and **5** the solvent molecules occupy three positions in the upper square face (Figure 4d,e).

The three anilato ligands also occupy different positions in the coordination environment (Figure 4a–e) resulting in different spatial orientations of the anilato ligands that lead to very different distortions of the hexagonal cavities (Figure 4f–j).

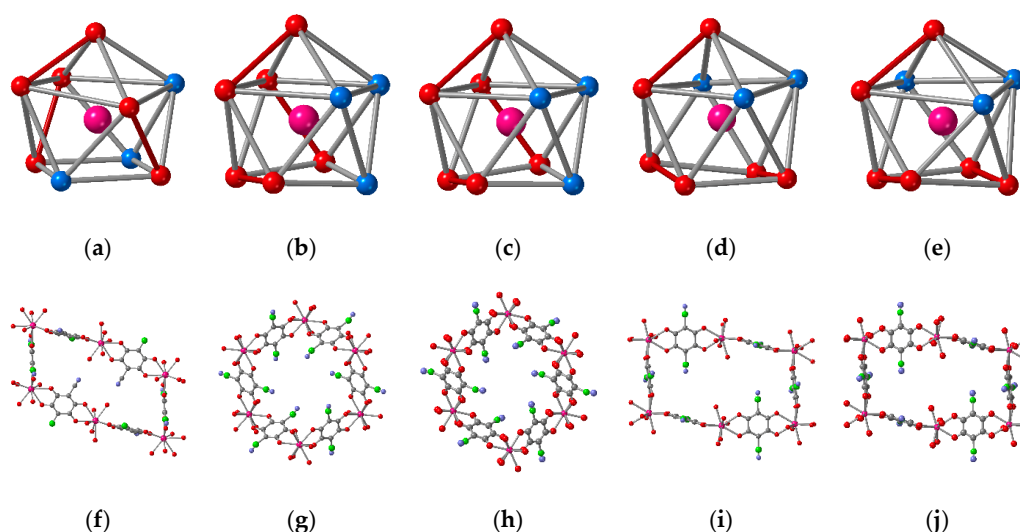


**Figure 4.** (a–e) Coordination polyhedra of the Ln(III) ions in compounds 1–5, respectively. The red lines correspond to the three chelating chlorocyananilato ligands. (f–j) Cavities in compounds 1–5, respectively. Colour code in (a–e): Ln = pink,  $O_{\text{anilato}}$  = red and  $O_{\text{solvent}}$  = blue. Colour code in (f–j): Ln = pink, Cl = green, C = grey, O = red, N = dark blue. H atoms have been omitted for clarity.

Thus, in compounds 1, 4, 5 and in the previously reported  $[\text{Pr}_2(\text{C}_6\text{O}_4(\text{CN})\text{Cl})_3(\text{DMF})_6]$  (II) and  $[\text{Pr}_2(\text{C}_6\text{O}_4(\text{CN})\text{Cl})_3(\text{DMSO})_6]$  (III) [39], the cavities contain four anilato ligands whose ring planes are orthogonal to the cavity plane (edge-on, E) and two whose ring planes are parallel to the cavity plane (face-on, F), resulting in a rectangular shape. In contrast, in compounds 2 and 3 and in the previously reported  $[\text{Ce}_2(\text{C}_6\text{O}_4(\text{CN})\text{Cl})_3(\text{DMF})_6] \cdot 2\text{H}_2\text{O}$  (I) and  $[\text{Yb}_2(\text{C}_6\text{O}_4(\text{CN})\text{Cl})_3(\text{DMSO})_4] \cdot 2\text{H}_2\text{O}$  (IV) [39], the six ligands have the same orientation and are tilted with respect to the cavity plane, resulting in quite regular hexagonal cavities. The most evident consequence of the change in the shape of the cavities is the presence or not of crystallization water molecules inside no matter the solvent used (DMF or DMSO). Thus, the compounds with hexagonal cavities (2, 3, I and IV) contain two or four crystallization water molecules, whereas the compounds with rectangular cavities (1, 4, 5, II and III) do not contain water molecules, as a consequence of the larger size of the hexagonal cavities.

In order to study the influence of the Ln(III) size, we first consider the series of five compounds prepared with the asymmetric chlorocyananilato ligand and DMF as solvent:  $[\text{Nd}_2(\text{C}_6\text{O}_4(\text{CN})\text{Cl})_3(\text{DMF})_6]$  (1),  $[\text{Dy}_2(\text{C}_6\text{O}_4(\text{CN})\text{Cl})_3(\text{DMF})_6] \cdot 4\text{H}_2\text{O}$  (2),  $[\text{Ho}_2(\text{C}_6\text{O}_4(\text{CN})\text{Cl})_3(\text{DMF})_6] \cdot 2\text{H}_2\text{O}$  (3) and the previously reported  $[\text{Ce}_2(\text{C}_6\text{O}_4(\text{CN})\text{Cl})_3(\text{DMF})_6] \cdot 2\text{H}_2\text{O}$  (I) and  $[\text{Pr}_2(\text{C}_6\text{O}_4(\text{CN})\text{Cl})_3(\text{DMF})_6]$  (II) [39]. In this series we can see up to three important structural changes as we move forward in the lanthanoids series: (i) the first change is observed when passing from Ce (compound I) to Pr (compound II) and implies a change from non-planar hexagonal cavities with the chair disposition in I to rectangular cavities with a spike disposition in II. (ii) A second structural change is observed between Pr (compound II) and Nd (compound 1) and implies a change from a rectangular spike-like layer in II to a rectangular brick wall one in 1. (iii) Finally, when passing from Nd (1) to Dy (2) and Ho (3) we observe a change from a rectangular brick wall layer in 1 to a hexagonal one in 2 and 3. Although the series is not complete yet, we can clearly see that the Ln(III) size is playing a key role in determining the size and shape of the cavities in the layered structures, while keeping the same (6,3)-2D topology. With the exception of the cerium compound (I), the larger ions (Pr and Nd) give rise to rectangular cavities whereas the smaller ions (Dy and Ho) give hexagonal cavities. Further experiments are in progress in order to determine the reason for this anomaly of Ce.

Interestingly, the series of four compounds prepared with DMSO:  $[\text{Ce}_2(\text{C}_6\text{O}_4(\text{CN})\text{Cl})_3(\text{DMSO})_6]$  (4),  $[\text{Nd}_2(\text{C}_6\text{O}_4(\text{CN})\text{Cl})_3(\text{DMSO})_6]$  (5) and the previously reported  $[\text{Pr}_2(\text{C}_6\text{O}_4(\text{CN})\text{Cl})_3(\text{DMSO})_6]$  (III) and  $[\text{Yb}_2(\text{C}_6\text{O}_4(\text{CN})\text{Cl})_3(\text{DMSO})_4] \cdot 2\text{H}_2\text{O}$  (IV) [39], shows a similar effect: the larger ions (Ce, Pr and Nd) present rectangular cavities with no solvent molecules whereas the smaller ion (Yb) shows hexagonal cavities with two crystallization water molecules. In this last compound, the much smaller size of the Yb(III) ion has a second important effect: the reduction of the coordination number from nine to eight and, therefore, a change in the coordination geometry from capped square anti-prism to triangular dodecahedron [39].

## 2.6. Magnetic Properties

The product of the molar magnetic susceptibility times the temperature ( $\chi_m T$ ) per formula (two Ln(III) ions) in compounds  $[\text{Nd}_2(\text{C}_6\text{O}_4(\text{CN})\text{Cl})_3(\text{DMF})_6]$  (1),  $[\text{Dy}_2(\text{C}_6\text{O}_4(\text{CN})\text{Cl})_3(\text{DMF})_6] \cdot 4\text{H}_2\text{O}$  (2),  $[\text{Ho}_2(\text{C}_6\text{O}_4(\text{CN})\text{Cl})_3(\text{DMF})_6] \cdot 2\text{H}_2\text{O}$  (3),  $[\text{Ce}_2(\text{C}_6\text{O}_4(\text{CN})\text{Cl})_3(\text{DMSO})_6]$  (4) and  $[\text{Nd}_2(\text{C}_6\text{O}_4(\text{CN})\text{Cl})_3(\text{DMSO})_6]$  (5) is ca. 3.3, 28.8, 28.8, 1.6 and 3.2  $\text{cm}^3 \text{K mol}^{-1}$ , respectively. These values are close to the expected ones for the corresponding Ln(III) ions (Table 4, Figure 5) [46]. When the samples are cooled, the  $\chi_m T$  product decreases from room temperature in compounds 1, 4 and 5 to reach values of 1.45, 0.38 and 1.20  $\text{cm}^3 \text{K mol}^{-1}$  at 2 K, respectively (Figure 5). The  $\chi_m T$  value in compounds 2 and 3 remains constant from room temperature down to ca. 50 K in 2 and ca. 120 K in 3 and show a progressive decrease at lower temperatures to reach values of 24.1 and 8.3  $\text{cm}^3 \text{K mol}^{-1}$  at 2 K, respectively. The decrease observed in all the compounds at low temperature can be attributed to the depopulation of the high energy sublevels that appear due to the splitting of the ground levels caused by the ligand field effects. Note that the decrease might also include a very weak, although negligible, antiferromagnetic Ln-Ln coupling through the chlorocyananilato bridge.

**Table 4.** Magnetic properties of compounds  $[\text{Nd}_2(\text{C}_6\text{O}_4(\text{CN})\text{Cl})_3(\text{DMF})_6]$  (1),  $[\text{Dy}_2(\text{C}_6\text{O}_4(\text{CN})\text{Cl})_3(\text{DMF})_6] \cdot 4\text{H}_2\text{O}$  (2),  $[\text{Ho}_2(\text{C}_6\text{O}_4(\text{CN})\text{Cl})_3(\text{DMF})_6] \cdot 2\text{H}_2\text{O}$  (3) and  $[\text{Ln}_2(\text{C}_6\text{O}_4(\text{CN})\text{Cl})_3(\text{DMSO})_6]$  with Ln = Ce (4) and Nd (5).

Compound	$\chi_m T_{\text{experimental}}^a$ ( $\text{cm}^3 \text{K mol}^{-1}$ )	g	S	L	J	$\chi_m T_{\text{calculated}}$ ( $\text{cm}^3 \text{K mol}^{-1}$ )
$[\text{Nd}_2(\text{C}_6\text{O}_4(\text{CN})\text{Cl})_3(\text{DMF})_6]$ (1)	1.65	8/11	3/2	6	9/2	1.64
$[\text{Dy}_2(\text{C}_6\text{O}_4(\text{CN})\text{Cl})_3(\text{DMF})_6] \cdot 4\text{H}_2\text{O}$ (2)	14.4	4/3	5/2	5	15/2	14.17
$[\text{Ho}_2(\text{C}_6\text{O}_4(\text{CN})\text{Cl})_3(\text{DMF})_6] \cdot 2\text{H}_2\text{O}$ (3)	14.4	5/4	2	6	8	14.07
$[\text{Ce}_2(\text{C}_6\text{O}_4(\text{CN})\text{Cl})_3(\text{DMSO})_6]$ (4)	0.8	6/7	1/2	3	5/2	0.80
$[\text{Nd}_2(\text{C}_6\text{O}_4(\text{CN})\text{Cl})_3(\text{DMSO})_6]$ (5)	1.6	8/11	3/2	6	9/2	1.64

<sup>a</sup> Value per Ln(III) ion.

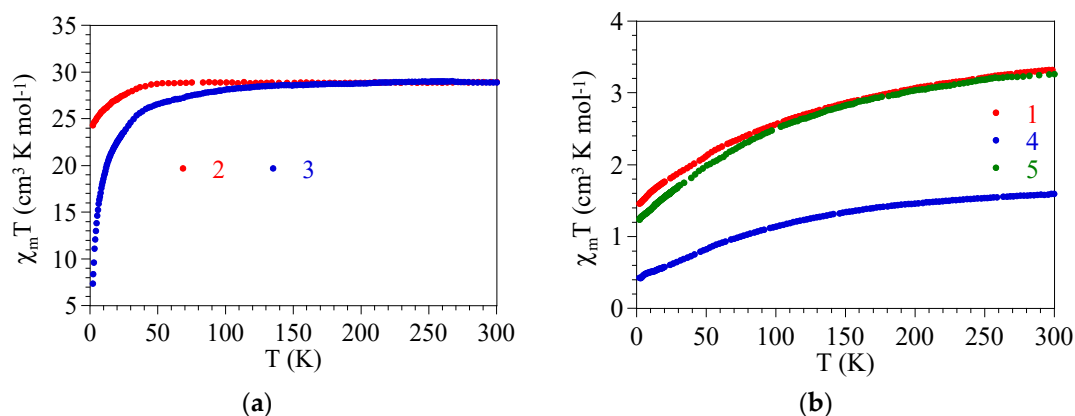


**Figure 5.** Thermal variation of the  $\chi_m T$  product for compounds (a) 1, 4 and 5 and (b) 2 and 3.

The observed behaviour indicates that all compounds are paramagnetic and, therefore, that the chlorocyananilato bridge does not originate any noticeable magnetic coupling, as observed in all the reported compounds with this ligand and Ln(III) ions [36–39]. This magnetic isolation represents an advantage for the preparation of Ln-based single molecule magnets (SMM) in these series of compounds by simply diluting the paramagnetic centres with diamagnetic lanthanoids as La(III) and Eu(III). In fact, our preliminary results indicate that it is possible to obtain SMM and field-induced SMM using this very simple strategy and taking advantage of the isostructurality of many of these compounds.

### 3. Experimental Section

#### 3.1. Starting Materials

The Ln(III) nitrates  $\text{Nd}(\text{NO}_3)_3 \cdot 6\text{H}_2\text{O}$ ,  $\text{Dy}(\text{NO}_3)_3 \cdot 5\text{H}_2\text{O}$ ,  $\text{Ho}(\text{NO}_3)_3 \cdot 5\text{H}_2\text{O}$  and  $\text{Ce}(\text{NO}_3)_3 \cdot 6\text{H}_2\text{O}$  as well as all the solvents used in this work, are commercially available and were used as received. The chlorocyananilato ligand, as  $[\text{Ph}_4\text{P}]_2[\text{C}_6\text{O}_4(\text{CN})\text{Cl}] \cdot 2\text{H}_2\text{O}$  or  $\text{KH}[\text{C}_6\text{O}_4(\text{CN})\text{Cl}]$ , was prepared following the literature [47].

#### 3.2. Synthesis of $[\text{Nd}_2(\text{C}_6\text{O}_4(\text{CN})\text{Cl})_3(\text{DMF})_6]$ (1)

Compound **1** was obtained as single crystals by carefully layering, at room temperature, a solution of  $[\text{Ph}_4\text{P}]_2[\text{C}_6\text{O}_4(\text{CN})\text{Cl}] \cdot 2\text{H}_2\text{O}$  (18.25 mg, 0.02 mmol) in 5 mL of methanol, on top of a solution of  $\text{Nd}(\text{NO}_3)_3 \cdot 6\text{H}_2\text{O}$  (8.77 mg, 0.02 mmol) in 5 mL of dimethylformamide (DMF). The tube was sealed and allowed to stand for about two months to obtain purple block-shaped single crystals suitable for X-ray diffraction. Yield: 3.15 mg (24%). The IR spectrum and the assignment of the main bands are included in the supporting information (Figure S6 and Table S1).

#### 3.3. Synthesis of $[\text{Dy}_2(\text{C}_6\text{O}_4(\text{CN})\text{Cl})_3(\text{DMF})_6] \cdot 4\text{H}_2\text{O}$ (2)

Compound **2** was obtained as single crystals by carefully layering, at room temperature, a solution of  $[\text{Ph}_4\text{P}]_2[\text{C}_6\text{O}_4(\text{CN})\text{Cl}] \cdot 2\text{H}_2\text{O}$  (18.25 mg, 0.02 mmol) in 5 mL of methanol, on top of a solution of  $\text{Dy}(\text{NO}_3)_3 \cdot 5\text{H}_2\text{O}$  (8.77 mg, 0.02 mmol) in 5 mL of DMF. The tube was sealed and allowed to stand for about one month to obtain red prismatic single crystals suitable for X-ray diffraction. Yield: 2.33 mg (16%). The IR spectrum and the assignment of the main bands are included in the supporting information (Figure S7 and Table S1).

#### 3.4. Synthesis of $[\text{Ho}_2(\text{C}_6\text{O}_4(\text{CN})\text{Cl})_3(\text{DMF})_6] \cdot 2\text{H}_2\text{O}$ (3)

Compound **3** was obtained as single crystals by carefully layering, at room temperature, a solution of  $\text{Ho}(\text{NO}_3)_3 \cdot 5\text{H}_2\text{O}$  (8.82 mg, 0.02 mmol) in 5 mL of methanol, on top of a solution of  $\text{KH}[\text{C}_6\text{O}_4(\text{CN})\text{Cl}]$  (4.75 mg, 0.02 mmol) in 5 mL of DMF. The tube was sealed and allowed to stand for about one month to obtain red block-shaped single crystals suitable for X-ray diffraction. Yield: 1.55 mg (11%). The IR spectrum and the assignment of the main bands are included in the supporting information (Figure S8 and Table S1).

#### 3.5. Synthesis of $[\text{Ce}_2(\text{C}_6\text{O}_4(\text{CN})\text{Cl})_3(\text{DMSO})_6]$ (4)

Compound **4** was obtained as single crystals by carefully layering, at room temperature, a solution of  $\text{Ce}(\text{NO}_3)_3 \cdot 6\text{H}_2\text{O}$  (8.68 mg, 0.02 mmol) in 5 mL of methanol, on top of a solution of  $\text{KH}[\text{C}_6\text{O}_4(\text{CN})\text{Cl}]$  (4.75 mg, 0.02 mmol) in 5 mL of dimethylsulfoxide (DMSO). The tube was sealed and allowed to stand for about five months to obtain purple rhombohedral single crystals suitable for X-ray diffraction. Yield: 2.83 mg (21%). The IR spectrum and the assignment of the main bands are included in the supporting information (Figure S9 and Table S1).

### 3.6. Synthesis of $[Nd_2(C_6O_4(CN)Cl)_3(DMSO)_6]$ (**5**)

Compound **5** was obtained as single crystals by carefully layering, at room temperature, a solution of  $Nd(NO_3)_3 \cdot 6H_2O$  (8.77 mg, 0.02 mmol) in 5 mL of methanol, on top of a solution of  $KH[C_6O_4(CN)Cl]$  (4.75 mg, 0.02 mmol) in 5 mL of DMSO. The tube was sealed and allowed to stand for about one month to obtain orange block-shaped single crystals suitable for X-ray diffraction. Yield: 5.50 mg (41%). The IR spectrum and the assignment of the main bands are included in the supporting information (Figure S10 and Table S1).

### 3.7. Magnetic Measurements

Magnetic susceptibility measurements were carried out in the temperature range 2–300 K with an applied magnetic field of 0.5 T on polycrystalline samples of compounds **1–5** with a Quantum Design MPMS-XL-5 SQUID susceptometer (San Diego, CA, USA). The susceptibility data were corrected for the sample holders previously measured using the same conditions and for the diamagnetic contributions of the salt as deduced by using Pascal's constant tables [48].

### 3.8. Crystallographic Data Collection and Refinement

Suitable single crystals of compounds **1–5** were manually mounted in a loop using a viscous hydrocarbon oil and transferred directly to the cold nitrogen stream for data collection. Since compounds **2** and **3** show a very fast loss of crystallinity, single crystals of these compounds were extracted from their solutions immediately before their use. X-ray data were collected at 120 K on a Supernova diffractometer equipped with a graphite monochromated Enhance (Mo) X-ray Source ( $\lambda = 0.71073 \text{ \AA}$ ). Unit cell determinations and data reduction was performed with the program CrysAlisPro, Oxford Diffraction Ltd. [49]. Empirical absorption correction was performed using spherical harmonics, implemented in the SCALE3 ABSPACK scaling algorithm. Compounds **1**, **4** and **5** crystallize in the monoclinic  $P2_1/n$  space group and compounds **2** and **3** in the monoclinic  $C2/c$  space group (Table 1). Crystal structures were solved and refined against all  $F^2$  values with the SHELXL-2014 program [50], using the WinGX2014.1 graphical user interface [51]. Non-hydrogen atoms were refined anisotropically and hydrogen atoms were assigned fixed isotropic displacement parameters. Hydrogen atoms associated with oxygen atoms were located from the difference map and the O-H distance fixed at 0.86  $\text{\AA}$ . Table 1 displays a summary of the data collection and structure refinements for compounds **1–5**.

CCDC-1877130-4 contain the supplementary crystallographic data for compounds **1–5**, respectively. These data can be obtained free of charge from The Cambridge Crystallographic Data Centre at [www.ccdc.cam.ac.uk/data\\_request/cif](http://www.ccdc.cam.ac.uk/data_request/cif).

### 3.9. X-ray Powder Diffraction

The X-ray powder diffractograms were collected for of all compounds (using the same polycrystalline samples used for the magnetic measurements) with a 0.5 mm glass capillary that was mounted and aligned on a Empyrean PANalytical powder diffractometer, using  $CuK\alpha$  radiation ( $\lambda = 1.54177 \text{ \AA}$ ). A total of 3 or 6 scans were collected at room temperature in the  $2\theta$  range 2–40°. The partial loss of crystallinity of samples **2** and **3** is attributed to the loss of solvent molecules during the storage and magnetic measurements.

### 3.10. IR Spectroscopy

FT-IR spectra were performed on KBr pellets and collected with a Nexus-Nicolet 5700 spectrophotometer in the range 400–4000  $\text{cm}^{-1}$ .

#### 4. Conclusions

The combination of different Ln(III) ions as Nd, Dy, Ho and Ce with the asymmetric anilato derivative ligand chlorocyananilato and using DMF and DMSO as coordinating solvents, have led to the formation of five new compounds formulated as:  $[\text{Nd}_2(\text{C}_6\text{O}_4(\text{CN})\text{Cl})_3(\text{DMF})_6]$  (**1**),  $[\text{Dy}_2(\text{C}_6\text{O}_4(\text{CN})\text{Cl})_3(\text{DMF})_6] \cdot 4\text{H}_2\text{O}$  (**2**),  $[\text{Ho}_2(\text{C}_6\text{O}_4(\text{CN})\text{Cl})_3(\text{DMF})_6] \cdot 2\text{H}_2\text{O}$  (**3**) and  $[\text{Ln}_2(\text{C}_6\text{O}_4(\text{CN})\text{Cl})_3(\text{DMSO})_6]$  with Ln = Ce (**4**) and Nd (**5**). All compounds show honeycomb (6,3)-2D lattices with quite regular hexagonal cavities in the compounds with small ions (Dy in **2** and Ho in **3**) and rectangular cavities in the compounds with large cations (Nd in **1** and **5** and Ce in **4**). A detailed analysis of the coordination geometry and of the positions occupied by the anilato ligands and the solvent molecules leads to the conclusion that the spatial disposition of the ligands around the Ln(III) ion determines the shape and distortion of the cavities, since in all compounds the coordination geometry is the same (capped square anti-prism). This aspect is important since the hexagonal cavities contain additional water crystallization molecules but the rectangular ones do not have enough free space to accommodate any water molecules.

The synthesis of the complete Ln(III) series with this ligand and these and other solvents is under investigation in order to elucidate the role played by the size and shape of the solvent and by the size of the Ln(III) ions in their final structures and properties. The luminescent properties of these compounds are also under study since both, the Ln(III) ions and the asymmetric ligand chlorocyananilato, are good candidates to show luminescence.

**Supplementary Materials:** The following are available online at <http://www.mdpi.com/2312-7481/4/4/58/s1>, Figure S1: Experimental and simulated X-ray powder diffractograms for compound  $[\text{Nd}_2(\text{C}_6\text{O}_4(\text{CN})\text{Cl})_3(\text{DMF})_6]$  (**1**), Figure S2: Experimental and simulated X-ray powder diffractograms for compound  $[\text{Dy}_2(\text{C}_6\text{O}_4(\text{CN})\text{Cl})_3(\text{DMF})_6] \cdot 4\text{H}_2\text{O}$  (**2**), Figure S3: Experimental and simulated X-ray powder diffractograms for compound  $[\text{Ho}_2(\text{C}_6\text{O}_4(\text{CN})\text{Cl})_3(\text{DMF})_6] \cdot 2\text{H}_2\text{O}$  (**3**), Figure S4: Experimental and simulated X-ray powder diffractograms for compound  $[\text{Ce}_2(\text{C}_6\text{O}_4(\text{CN})\text{Cl})_3(\text{DMSO})_6]$  (**4**), Figure S5: Experimental and simulated X-ray powder diffractograms for compound  $[\text{Nd}_2(\text{C}_6\text{O}_4(\text{CN})\text{Cl})_3(\text{DMSO})_6]$  (**5**), Figure S6: IR spectrum of compound  $[\text{Nd}_2(\text{C}_6\text{O}_4(\text{CN})\text{Cl})_3(\text{DMF})_6]$  (**1**) in (a) the 4000–400  $\text{cm}^{-1}$  and (b) 2000–400  $\text{cm}^{-1}$  ranges, Figure S7: IR spectrum of compound  $[\text{Dy}_2(\text{C}_6\text{O}_4(\text{CN})\text{Cl})_3(\text{DMF})_6] \cdot 4\text{H}_2\text{O}$  (**2**) in (a) the 4000–400  $\text{cm}^{-1}$  and (b) 2000–400  $\text{cm}^{-1}$  ranges, Figure S8: IR spectrum of compound  $[\text{Ho}_2(\text{C}_6\text{O}_4(\text{CN})\text{Cl})_3(\text{DMF})_6] \cdot 2\text{H}_2\text{O}$  (**3**) in (a) the 4000–400  $\text{cm}^{-1}$  and (b) 2000–400  $\text{cm}^{-1}$  ranges, Figure S9: IR spectrum of compound  $[\text{Ce}_2(\text{C}_6\text{O}_4(\text{CN})\text{Cl})_3(\text{DMSO})_6]$  (**4**) in (a) the 4000–400  $\text{cm}^{-1}$  and (b) 2000–400  $\text{cm}^{-1}$  ranges, Figure S10: IR spectrum of compound  $[\text{Nd}_2(\text{C}_6\text{O}_4(\text{CN})\text{Cl})_3(\text{DMSO})_6]$  (**5**) in (a) the 4000–400  $\text{cm}^{-1}$  and (b) 2000–400  $\text{cm}^{-1}$  ranges, Table S1: Main IR bands ( $\text{cm}^{-1}$ ) and their assignment in compounds  $[\text{Nd}_2(\text{C}_6\text{O}_4(\text{CN})\text{Cl})_3(\text{DMF})_6]$  (**1**)  $[\text{Dy}_2(\text{C}_6\text{O}_4(\text{CN})\text{Cl})_3(\text{DMF})_6] \cdot 4\text{H}_2\text{O}$  (**2**),  $[\text{Ho}_2(\text{C}_6\text{O}_4(\text{CN})\text{Cl})_3(\text{DMF})_6] \cdot 2\text{H}_2\text{O}$  (**3**), and  $[\text{Ln}_2(\text{C}_6\text{O}_4(\text{CN})\text{Cl})_3(\text{DMSO})_6]$  with Ln = Ce (**4**) and Nd (**5**).

**Author Contributions:** S.B. designed the synthesis, performed the X-ray structural analysis and supervised all the experiments. A.H.-P. performed the synthesis of the ligand and of the compounds. C.J.G.-G. performed the magnetic measurements and supervised all the experiments. All the authors contributed to the writing of the manuscript.

**Funding:** This research was funded by the Generalitat Valenciana (Prometeo2014/II/076 project) and the Spanish MINECO (Project CTQ2017-87201-P AEI/FEDER, EU).

**Acknowledgments:** A.H.-P. thanks the Spanish MINECO for a pre-doctoral grant (FPU Program).

**Conflicts of Interest:** The authors declare no conflict of interest.

#### References

1. Zhou, H.C.; Long, J.R.; Yaghi, O.M. Introduction to metal-organic frameworks. *Chem. Rev.* **2012**, *112*, 673–674. [[CrossRef](#)] [[PubMed](#)]
2. Furukawa, H.; Cordova, K.E.; O’Keeffe, M.; Yaghi, O.M. The chemistry and applications of metal-organic frameworks. *Science* **2013**, *341*, 1230444. [[CrossRef](#)] [[PubMed](#)]
3. Nandasiri, M.I.; Jambovane, S.R.; McGrail, B.P.; Schaefer, H.T.; Nune, S.K. Adsorption, separation, and catalytic properties of densified metal-organic frameworks. *Coord. Chem. Rev.* **2016**, *311*, 38–52. [[CrossRef](#)]
4. Huang, Y.B.; Liang, J.; Wang, X.S.; Cao, R. Multifunctional metal-organic framework catalysts: Synergistic catalysis and tandem reactions. *Chem. Soc. Rev.* **2017**, *46*, 126–157. [[CrossRef](#)] [[PubMed](#)]

5. Barea, E.; Montoro, C.; Navarro, J.A. Toxic gas removal-Metal-organic frameworks for the capture and degradation of toxic gases and vapours. *Chem. Soc. Rev.* **2014**, *43*, 5419–5430. [[CrossRef](#)] [[PubMed](#)]
6. Schoedel, A.; Ji, Z.; Yaghi, O.M. The role of metal-organic frameworks in a carbon-neutral energy cycle. *Nat. Energy* **2016**, *1*, 16034. [[CrossRef](#)]
7. Wang, L.; Han, Y.; Feng, X.; Zhou, J.; Qi, P.; Wang, B. Metal-organic frameworks for energy storage: Batteries and supercapacitors. *Coord. Chem. Rev.* **2016**, *307*, 361–381. [[CrossRef](#)]
8. Bai, S.; Liu, X.; Zhu, K.; Wu, S.; Zhou, H. Metal-organic framework-based separator for lithium-sulfur batteries. *Nat. Energy* **2016**, *1*, 16094. [[CrossRef](#)]
9. Canivet, J.; Fateeva, A.; Guo, Y.; Coasne, B.; Farrusseng, D. Water adsorption in MOFs: Fundamentals and applications. *Chem. Soc. Rev.* **2014**, *43*, 5594–5617. [[CrossRef](#)]
10. Horcajada, P.; Gref, R.; Baati, T.; Allan, P.K.; Maurin, G.; Couvreur, P.; Ferey, G.; Morris, R.E.; Serre, C. Metal-organic frameworks in biomedicine. *Chem. Rev.* **2012**, *112*, 1232–1268. [[CrossRef](#)]
11. Wu, M.X.; Yang, Y.W. Metal-Organic Framework (MOF)-Based Drug/Cargo Delivery and Cancer Therapy. *Adv. Mater.* **2017**, *29*, 1606134. [[CrossRef](#)] [[PubMed](#)]
12. Kreno, L.E.; Leong, K.; Farha, O.K.; Allendorf, M.; Van Duyne, R.P.; Hupp, J.T. Metal-organic framework materials as chemical sensors. *Chem. Rev.* **2012**, *112*, 1105–1125. [[CrossRef](#)] [[PubMed](#)]
13. Campbell, M.G.; Dinca, M. Metal-Organic Frameworks as Active Materials in Electronic Sensor Devices. *Sensors* **2017**, *17*, 1108. [[CrossRef](#)] [[PubMed](#)]
14. Li, B.; Wen, H.M.; Cui, Y.; Zhou, W.; Qian, G.; Chen, B. Emerging Multifunctional Metal-Organic Framework Materials. *Adv. Mater.* **2016**, *28*, 8819–8860. [[CrossRef](#)] [[PubMed](#)]
15. Fordham, S.; Wang, X.; Bosch, M.; Zhou, H. Lanthanide Metal-Organic Frameworks: Syntheses, Properties, and Potential Applications. *Struct. Bond.* **2015**, *163*, 1–27.
16. Wang, C.; Liu, X.; Keser Demir, N.; Chen, J.P.; Li, K. Applications of water stable metal-organic frameworks. *Chem. Soc. Rev.* **2016**, *45*, 5107–5134. [[CrossRef](#)] [[PubMed](#)]
17. Liu, X.; Fu, W.; Bouwman, E. One-step growth of lanthanoid metal-organic framework (MOF) films under solvothermal conditions for temperature sensing. *Chem. Commun.* **2016**, *52*, 6926–6929. [[CrossRef](#)] [[PubMed](#)]
18. Zhang, W.; Zhang, W.; Wang, R.; Ren, C.; Li, Q.; Fan, Y.; Liu, B.; Liu, P.; Wang, Y. Effect of Coordinated Solvent Molecules on Metal Coordination Sphere and Solvent-Induced Transformations. *Cryst. Growth Des.* **2017**, *17*, 517–526. [[CrossRef](#)]
19. Li, X.; Sun, X.; Li, X.; Fu, Z.; Su, Y.; Xu, G. Porous Cadmium(II) Anionic Metal-Organic Frameworks Based on Aromatic Tricarboxylate Ligands: Encapsulation of Protonated Flexible Bis(2-methylimidazolyl) Ligands and Proton Conductivity. *Cryst. Growth Des.* **2015**, *15*, 4543–4548. [[CrossRef](#)]
20. Sun, L.; Qi, Y.; Che, Y.; Batten, S.R.; Zheng, J. Three Unprecedented Entangled Metal-Organic Frameworks: Self-Penetration and Hydrothermal in Situ Ligand Formation. *Cryst. Growth Des.* **2009**, *9*, 2995–2998. [[CrossRef](#)]
21. Zhao, D.; Timmons, D.J.; Yuan, D.; Zhou, H.C. Tuning the topology and functionality of metal-organic frameworks by ligand design. *Acc. Chem. Res.* **2011**, *44*, 123–133. [[CrossRef](#)] [[PubMed](#)]
22. Banerjee, R.; Phan, A.; Wang, B.; Knobler, C.; Furukawa, H. High-Throughput Synthesis of Zeolitic Imidazolate Frameworks and Application to CO<sub>2</sub> Capture. *Science* **2008**, *319*, 939–943. [[CrossRef](#)] [[PubMed](#)]
23. Zhang, J.P.; Zhang, Y.B.; Lin, J.B.; Chen, X.M. Metal azolate frameworks: From crystal engineering to functional materials. *Chem. Rev.* **2012**, *112*, 1001–1033. [[CrossRef](#)] [[PubMed](#)]
24. Kitagawa, S.; Kawata, S. Coordination compounds of 1,4-dihydroxybenzoquinone and its homologues. Structures and properties. *Coord. Chem. Rev.* **2002**, *224*, 11–34. [[CrossRef](#)]
25. Mercuri, M.L.; Congiu, F.; Concas, G.; Sahadevan, S.A. Recent Advances on Anilato-Based Molecular Materials with Magnetic and/or Conducting Properties. *Magnetochemistry* **2017**, *3*, 17. [[CrossRef](#)]
26. Atzori, M.; Artizzu, F.; Sessini, E.; Marchio, L.; Loche, D.; Serpe, A.; Deplano, P.; Concas, G.; Pop, F.; Avarvari, N.; et al. Halogen-bonding in a new family of tris(haloanilato)metallate(III) magnetic molecular building blocks. *Dalton Trans.* **2014**, *43*, 7006–7019. [[CrossRef](#)] [[PubMed](#)]
27. Benmansour, S.; Gómez-Claramunt, P.; Vallés-García, C.; Mínguez Espallargas, G.; Gómez García, C.J. Key Role of the Cation in the Crystallization of Chiral Tris(Anilato)Metalate Magnetic Anions. *Cryst. Growth Des.* **2016**, *16*, 518–526. [[CrossRef](#)]
28. Abrahams, B.F.; Coleiro, J.; Ha, K.; Hoskins, B.F.; Orchard, S.D.; Robson, R. Dihydroxybenzoquinone and chloranilic acid derivatives of rare earth metals. *J. Chem. Soc. Dalton Trans.* **2002**, *8*, 1586–1594. [[CrossRef](#)]

29. Abrahams, B.F.; Hudson, T.A.; McCormick, L.J.; Robson, R. Coordination polymers of 2,5-dihydroxybenzoquinone and chloranilic acid with the (10,3)-a Topology. *Cryst. Growth Des.* **2011**, *11*, 2717–2720. [[CrossRef](#)]
30. Atzori, M.; Benmansour, S.; Mínguez Espallargas, G.; Clemente-León, M.; Abhervé, A.; Gómez-Claramunt, P.; Coronado, E.; Artizzu, F.; Sessini, E.; Deplano, P.; et al. A Family of Layered Chiral Porous Magnets Exhibiting Tunable Ordering Temperatures. *Inorg. Chem.* **2013**, *52*, 10031–10040. [[CrossRef](#)] [[PubMed](#)]
31. Benmansour, S.; Vallés-García, C.; Gómez-Claramunt, P.; Mínguez Espallargas, G.; Gómez-García, C.J. 2D and 3D Anilato-Based Heterometallic M(I)M(III) Lattices: The Missing Link. *Inorg. Chem.* **2015**, *54*, 5410–5418. [[CrossRef](#)] [[PubMed](#)]
32. Benmansour, S.; Gómez-García, C.J. A Heterobimetallic Anionic 3,6-Connected 2D Coordination Polymer Based on Nitranilate as Ligand. *Polymers* **2016**, *8*, 89. [[CrossRef](#)]
33. Benmansour, S.; Abhervé, A.; Gómez-Claramunt, P.; Vallés-García, C.; Gómez-García, C.J. Nanosheets of Two-Dimensional Magnetic and Conducting Fe(II)/Fe(III) Mixed-Valence Metal-Organic Frameworks. *ACS Appl. Mater. Interfaces* **2017**, *9*, 26210–26218. [[CrossRef](#)] [[PubMed](#)]
34. Jeon, I.; Negru, B.; Duyne, R.P.V.; Harris, T.D. A 2D Semiquinone Radical-Containing Microporous Magnet with Solvent-Induced Switching from  $T_c = 26$  to 80 K. *J. Am. Chem. Soc.* **2015**, *137*, 15699–15702. [[CrossRef](#)] [[PubMed](#)]
35. Abrahams, B.F.; Coleiro, J.; Hoskins, B.F.; Robson, R. Gas hydrate-like pentagonal dodecahedral  $M_2(H_2O)_{18}$  cages ( $M =$  lanthanide or Y) in 2,5-dihydroxybenzoquinone-derived coordination polymers. *Chem. Commun.* **1996**, 603–604. [[CrossRef](#)]
36. López-Martínez, G. Multifunctionality in Molecular Materials Based on Anilato-Type Ligands. Ph.D. Thesis, University of Valencia, València, Spain, 2017.
37. Benmansour, S.; Pérez-Herráez, I.; López-Martínez, G.; Gómez García, C.J. Solvent-modulated structures in anilato-based 2D coordination polymers. *Polyhedron* **2017**, *135*, 17–25. [[CrossRef](#)]
38. Benmansour, S.; López-Martínez, G.; Canet-Ferrer, J.; Gómez-García, C.J. A Family of Lanthanoid Dimers with Nitroanilato Bridges. *Magnetochemistry* **2016**, *2*, 3. [[CrossRef](#)]
39. Gómez-Claramunt, P.; Benmansour, S.; Hernández-Paredes, A.; Cerezo-Navarrete, C.; Rodríguez-Fernández, C.; Canet-Ferrer, J.; Cantarero, A.; Gómez-García, C.J. Tuning the Structure and Properties of Lanthanoid Coordination Polymers with an Asymmetric Anilato Ligand. *Magnetochemistry* **2018**, *4*, 6. [[CrossRef](#)]
40. Riley, P.E.; Haddad, S.F.; Raymond, K.N. Preparation of praseodymium(III) chloranilate and the crystal structures of  $Pr_2(C_6Cl_2O_4)_3 \cdot 8C_2H_5OH$  and  $Na_3[C_6H_2O(OH)(SO_3)_2] \cdot H_2O$ . *Inorg. Chem.* **1983**, *22*, 3090–3096.
41. Diaz-Torres, R.; Alvarez, S. Coordinating ability of anions and solvents towards transition metals and lanthanides. *Dalton Trans.* **2011**, *40*, 10742–10750. [[CrossRef](#)]
42. Benmansour, S.; Pérez-Herráez, I.; Cerezo-Navarrete, C.; López-Martínez, G.; Martínez Hernandez, C.; Gómez-García, C.J. Solvent-modulation of the structure and dimensionality in lanthanoid-anilato coordination polymers. *Dalton Trans.* **2018**, *47*, 6729–6741. [[CrossRef](#)] [[PubMed](#)]
43. Benmansour, S.; Hernández-Paredes, A.; Gómez-García, C.J. Effect of the lanthanoid-size on the structure of a series of lanthanoid-anilato 2-D lattices. *J. Coord. Chem.* **2018**, *71*, 845–863. [[CrossRef](#)]
44. Llunell, M.; Casanova, D.; Cirera, J.; Bofill, J.M.; Alemany, P.; Alvarez, S.; Pinsky, M.; Avnir, D. *SHAPE, version 2.3*; University of Barcelona: Barcelona, Spain, 2013.
45. Ruiz-Martínez, A.; Casanova, D.; Alvarez, S. Polyhedral Structures with an Odd Number of Vertices: Nine-Coordinate Metal Compounds. *Chem. Eur. J.* **2008**, *14*, 1291–1303. [[CrossRef](#)]
46. Sorace, L.; Gatteschi, D. *Electronic Structure and Magnetic Properties of Lanthanide Molecular Complexes*; Layfield, R.A., Murugesu, M., Eds.; Wiley-VCH: Weinheim, Germany, 2015; Volume 1, pp. 1–25.
47. Atzori, M.; Artizzu, F.; Marchio, L.; Loche, D.; Caneschi, A.; Serpe, A.; Delano, P.; Avarvari, N.; Mercuri, M.L. Switching-on luminescence in anilate-based molecular materials. *Dalton Trans.* **2015**, *44*, 15786–15802. [[CrossRef](#)] [[PubMed](#)]
48. Bain, G.A.; Berry, J.F. Diamagnetic corrections and Pascal's constants. *J. Chem. Educ.* **2008**, *85*, 532–536. [[CrossRef](#)]
49. *CrysAlisPro, Version 171.33.55*; Oxford Diffraction Ltd.: Oxford, UK, 2004.
50. Sheldrick, G.M. Crystal structure refinement with SHELXL. *Acta Cryst. C* **2015**, *71*, 3–8. [[CrossRef](#)] [[PubMed](#)]
51. Farrugia, L.J. WinGX and ORTEP for Windows: An update. *J. Appl. Cryst.* **2012**, *45*, 849–854. [[CrossRef](#)]

